Automated detection of chronic kidney disease using higher-order features and elongated quinary patterns from B-mode ultrasound images

Neural Computing and Applications

Automated Detection of Chronic Kidney Disease Using Higher Order Features and Elongated Quinary Patterns From B-Mode Ultrasound Images

--Manuscript Draft--

Manuscript Number:	
Full Title:	Automated Detection of Chronic Kidney Disease Using Higher Order Features and Elongated Quinary Patterns From B-Mode Ultrasound Images
Article Type:	S.I. : Computer aided Medical Diagnosis
Keywords:	chronic kidney disease, bispectrum, cumulants, elongated quinary pattern
Corresponding Author:	U Rajendra Acharya Ngee Ann Polytechnic Singapore, SINGAPORE
Corresponding Author Secondary Information:	
Corresponding Author's Institution:	Ngee Ann Polytechnic
Corresponding Author's Secondary Institution:	
First Author:	U Rajendra Acharya
First Author Secondary Information:	
Order of Authors:	U Rajendra Acharya
	Kristen M Meiburger, PhD
	Joel E W Koh
	Yuki Hagiwara
	Oh Shu Lih
	Sook Sam Leong
	Edward J Ciaccio
	Jeannie Hsiu Ding Wong
	Mohammad Nazri Md Shah
	Filippo Molinari
	Kwan Hoong Ng
Order of Authors Secondary Information:	
Funding Information:	
Abstract:	Chronic kidney disease (CKD) is a continuing loss of kidney function, and early detection of this disease is fundamental to halt its progression to end-stage disease. Numerous methods have been proposed to detect CKD, mainly focusing on classification based upon peripheral clinical parameters, quantitative ultrasound parameters that must be manually calculated, or on shear wave elastography. No studies have been found that detect the presence or absence of CKD based solely from one B-mode ultrasound image. In this work, we propose an automated system to detect chronic kidney disease utilizing only the automatic extraction of features from a B-mode ultrasound image of the kidney, with a database of 405 images. Higher order bispectrum and cumulants, and elongated quinary patterns, are extracted from each image to provide a final total of 24,480 features per image. These features were subjected to a locality sensitive discriminant analysis (LSDA) technique, which provides 30 LSDA coefficients. The coefficients were arranged according to their t-value and inserted into various classifiers, to yield the best diagnostic accuracy using the least number of features. The best performance was obtained using a support

	vector machine and a radial basis function, utilizing only 5 features, and resulting in an accuracy of 99.75%, and a sensitivity and specificity of 100% and 99.57%, respectively. Based upon these findings, it is evident that the technique accurately and automatically identifies subjects with and without CKD from B-mode ultrasound images.
Suggested Reviewers:	Hasan Mir Professor, American University of Sharjah hmir@aus.edu Subject Expert
	Sadasivan Puthusserypady Professor, Danmarks Tekniske Universitet spu@elektro.dtu.dk Subject Expert
	Paul Joseph Professor, National Institute of Technology Calicut paul@nitc.ac.in Subject Expert
	Toshiyo Tamura Professor, Chiba University tamurat@faculty.chiba-u.jp Subject Expert
	Mohammed Al-Rawi Professor, Jordan University rawi@ju.edu.jo Subject Expert
	Masaki Yoshida Yoshida Professor, University Osaka Electro-Communication University yoshida@isc.osakac.ac.jp Subject Expert

Automated Detection of Chronic Kidney Disease Using Higher Order Features and Elongated Quinary Patterns From B-Mode Ultrasound Images

U Rajendra Acharya[1,2,3,*], Kristen M Meiburger[4], Joel En Wei Koh[1], Yuki Hagiwara[1], Shu Lih Oh[1], Sook Sam Leong[5], Edward J Ciaccio[6], Jeannie Hsiu Ding Wong[5], Mohammad Nazri Md Shah[5], Filippo Molinari[4], Kwan Hoong Ng[5]

[1] Department of Electronics and Computer Engineering, Ngee Ann Polytechnic, Singapore.
[2] Department of Biomedical Engineering, School of Science and Technology, Singapore University of Social Sciences, Singapore.
[3] School of Medicine, Faculty of Health and Medical Sciences, Taylor's University, Subang Jaya, Malaysia.
[4] Department of Electronics and Telecommunications, Politecnico di Torino, Italy.
[5] Department of Biomedical Imaging, Faculty of Medicine, University of Malaya, 50603 Kuala Lumpur, Malaysia.
[6] Department of Medicine, Columbia University, New York, USA.
*Corresponding Author:
Postal Address: Department of Electronics and Computer Engineering, Ngee Ann Polytechnic, Singapore 599489.
Telephone: +65 6460 6135; Email Address: aru@np.edu.sg

Abstract

Chronic kidney disease (CKD) is a continuing loss of kidney function, and early detection of this disease is fundamental to halt its progression to end-stage disease. Numerous methods have been proposed to detect CKD, mainly focusing on classification based upon peripheral clinical parameters, quantitative ultrasound parameters that must be manually calculated, or on shear wave elastography. No studies have been found that detect the presence or absence of CKD based solely from one B-mode ultrasound image. In this work, we propose an automated system to detect chronic kidney disease utilizing only the automatic extraction of features from a B-mode ultrasound image of the kidney, with a database of 405 images. Higher order bispectrum and cumulants, and elongated quinary patterns, are extracted from each image to provide a final total of 24,480 features per image. These features were subjected to a locality sensitive discriminant analysis (LSDA) technique, which provides 30 LSDA coefficients. The

coefficients were arranged according to their t-value and inserted into various classifiers, to yield the best diagnostic accuracy using the least number of features. The best performance was obtained using a support vector machine and a radial basis function, utilizing only 5 features, and resulting in an accuracy of 99.75%, and a sensitivity and specificity of 100% and 99.57%, respectively. Based upon these findings, it is evident that the technique accurately and automatically identifies subjects with and without CKD from B-mode ultrasound images.

Keywords: chronic kidney disease, bispectrum, cumulants, elongated quinary pattern, locality sensitive discriminant analysis, ultrasound

1. Introduction

Chronic kidney disease (CKD) is a progressive loss of kidney function of at least three months' duration, whose main causes are primary renal disorder, diabetes, and hypertension. Regardless of the aetiology, CKD is defined by renal fibrosis, and is characterised by glomerulosclerosis and tubulointerstitial fibrosis [1]. As CKD progresses, it results in an extensive tissue scarring, which causes the impairment of normal kidney parenchyma. Figure 1 shows an illustration of a healthy and diseased CKD. The pathologic damage is irreversible and can lead to morbidity and mortality . The prevalence of CKD is increasing worldwide. The estimated prevalence of CKD in the U.S. was 16.8% in 2007, while in Asia the prevalence ranged from 12.1% to 17.5% (2009-2010) [2]. Hence, the early intervention of CKD is crucial so that appropriate treatments can be administered to reduce the development of end-stage disease, which is costly and difficult to manage.

In CKD, impairment of kidney morphology and function are closely related. As such, information on morphology and function are required for CKD diagnosis. Currently, the role of laboratory testing is to provide a surrogate marker to estimate renal function, which is

measured using the glomerular filtration rate (GFR). CKD is grouped into 5 severity-based stages according to the GFR, and presence of CKD is defined by a GFR of less than 60mL/min per 1.73 m^2. When the GFR is calculated from serum creatinine values, it is known as the estimated GFR (eGFR), which incorporates one of several formulas, such as MDRD eGFR, CKD-epi eGFR and Cockcroft-Gault Creatinine Clearance. Imaging predominantly provides structural information. Non-invasive imaging by ultrasound, magnetic resonance imaging (MRI), and computed tomography (CT) are helpful to reveal kidney morphology. These imaging modalities enable satisfactory visualization and evaluation of the urinary tract and extra renal pathologies affecting the kidneys. As such, other potential causes of CKD, such as urinary tract obstruction, can readily be identified. However, CT and MRI imaging present their own risks and downsides, including radiation exposure and potential renal damage from the administration of iodinated contrast medium in the case of CT scans, being expensive to perform, and in the case of MRI, having limited patient selection due to certain contraindications. Therefore, CT and MRI imaging, while informative in specific situations, are not commonly used in CKD diagnosis [3].

Renal ultrasound is considered as the imaging modality of choice for the evaluation of subjects with previously undiagnosed kidney dysfunction, due to its being radiation-free, the ease of imaging the kidney and of alterations of image aspect due to disease, and its low associated cost. Furthermore, kidney disease often results in smaller kidneys that have a higher echogenicity, making it possible to differentiate between those with acute kidney injury [1]. Parenchymal echogenicity is also a widely used marker to detect nephropathy. It is assessed by comparing the echogenicity of the kidney cortex with that of the adjacent liver or spleen echogenicity [4]. Some other important features that can be appreciated with B-mode ultrasound images of the kidney are the differentiation between intrinsic causes of kidney

disease and obstructive disease, and the identification of congenital or hereditary kidney disease.

Numerous studies have investigated the research topic concerning the correct prediction of CKD using advanced classification algorithms, but utilized other clinical variables extracted from the patient data, such as age, sex, weight, blood pressure, and creatinine, in order to predict the GFR values [5]. Other studies have focused upon quantitative ultrasound imaging and calculated parameters such as kidney length, cortical thickness, pixel intensity, and intrarenal artery peak systolic velocity, and have evaluated the differences in these parameters among mild, moderate and severe CKD [6]. Still other approaches focused instead on shear wave elastography to evaluate renal parenchymal stiffness [7], [8]. These investigations, however, either require substantial clinical data that may not always be available, they may require several ultrasound clinical parameters that must be calculated and reported manually, or they may require specific ultrasound devices that permit shear wave elastography analysis. It is therefore evident that there is a need for an automated system for correct prediction of CKD, using data that is readily collected and does not require manual intervention.

In this study, we present a completely automated system that classifies the presence or absence of chronic kidney disease based only upon the B-mode kidney ultrasound image. To date, this is the first work that presents CKD prediction based solely upon a single B-mode ultrasound image.

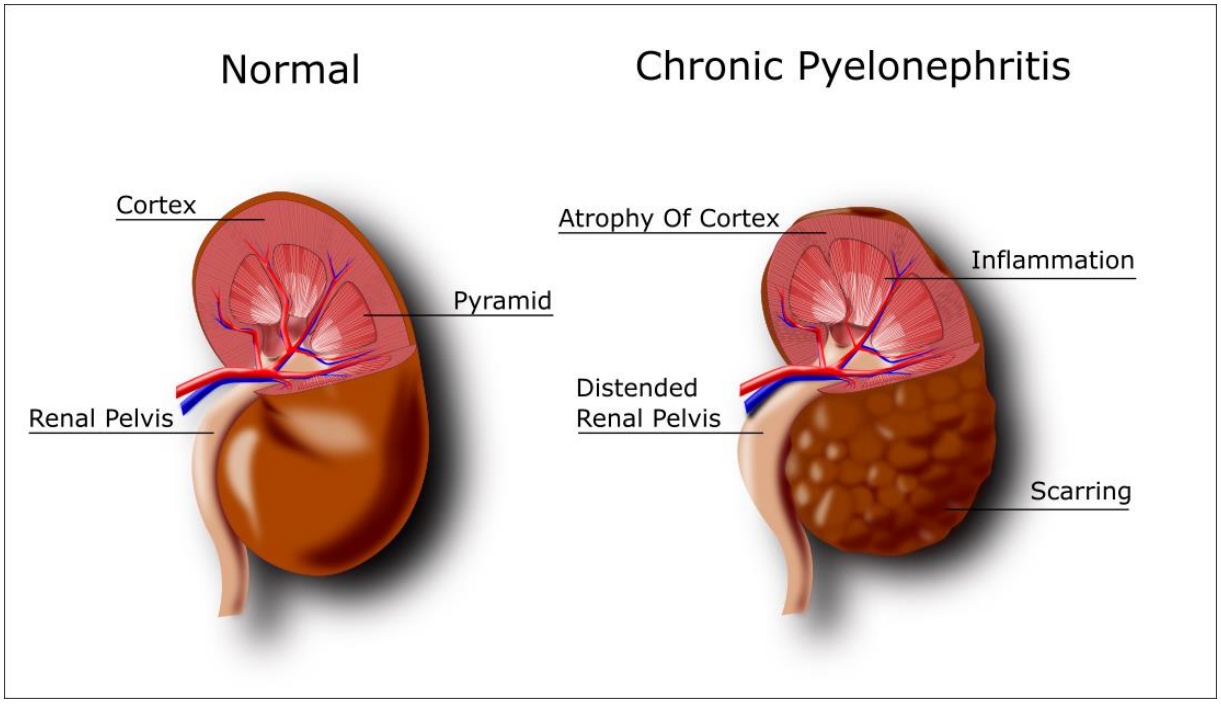

Figure 1. An illustration of the anatomy of a healthy and diseased kidney.

2. Materials and methods

In this section, each step of the developed system is described in-depth, as summarized in Figure 2.

Figure 2. The algorithm of the proposed technique.

2.1 Database

In this study, a total of N = 405 subjects was considered to validate the proposed system for diagnosis of chronic kidney disease from ultrasound images. 174 subjects were chronic kidney disease patients, whereas the remaining 231 subjects did not present any kidney disease. The images were acquired at the renal cortex, without the renal medulla and sinus, using an

ultrasound system. Local medical ethics approval was obtained from the Institutional Ethics Committee. The presence of chronic kidney disease was confirmed by the nephrologist. The 1st row of Figure 3 displays an example of a kidney ultrasound image for a subject with chronic kidney disease, versus a normal subject.

2.2 Preprocessing and Radon transform

As a first step, the ultrasound images are resized to a standard dimension of 512 × 512 pixels, and are then converted to grayscale. Next, an adaptive histogram equalization process was applied to the image [9] in order to enhance its visibility level. This was done by using local regions, termed tiles, within which the contrast is adaptively enhanced.

After this first preprocessing stage, the Radon transform (RT) was calculated. The RT performs image projection operations on the image, where the two-dimensional RT is the projection of the image intensity along a radial line that is oriented at a specific angle, generating a line integral which is the sum of the pixel intensities in each considered direction [10]. The RT can therefore capture directional features of an image and preserve intensity variations, preserving and boosting spatial-frequency information in the image. The RT was calculated every 2° from 0° to 178°, thereby providing 90 different angles, and therefore 90 different 1D RT sinogram signals.

2.3 Feature extraction

2.3.1 Bispectrum and cumulants

From the 1D RT sonogram signals (one signal for each considered angle), the higher-order bispectrum and cumulant features were extracted.

The spectral representations of higher order moments of a signal are known as higher order spectra [11], and the 3rd order statistic is known as the "bispectrum" , $B(x_1, x_2)$, or the Fourier transform of the 3rd order correlation, given by the averaged biperiodogram:

$$B(x_1, x_2) = E[F(x_1)F(x_2)F^*(x_1 + x_2)] \quad (1)$$

where $F(x)$ is the Fourier transform of the signal, * is the complex conjugation operator and $E[.]$ is the expectation operator, the average over a group of realizations of the random signal. Hence, the bispectrum is a function of two frequencies and exhibits symmetry (second row of Figure 3), being that the bispectrum of a real-valued signal is defined uniquely within the triangle $0 \leq x_2 \leq x_1 \leq x_1 + x_2 \leq 1$, assuming no bispectral aliasing [12].

Cumulants are higher-order statistics that have been substantially used in the biosignal processing field, given that first and second-order statistics are insufficient for representing nonlinear signals [13].

Thus, the first four order moments (m_n^F) can be calculated as follows:

$$m_1^F = E[F(n)]$$

$$m_2^F(i) = E[F(n)F(n+i)]$$

$$m_3^F(i,j) = E[F(n)F(n+i)F(n+j)]$$

$$m_4^F(i,j,k) = E[F(n)F(n+i)F(n+j)F(n+k)] \quad (2)$$

where $F(n)$ is assumed to be a zero-mean process. From these moments, it is therefore possible to compute the cumulants (C_n^F) as nonlinear combinations (3rd row of Figure 3). Here the first four order cumulants are defined:

$$C_1^F = m_1^F$$

$$C_2^F(i) = m_2^F(i)$$

$$C_3^F(i,j) = m_3^F(i,j)$$

$$C_4^F(i,j,k) = m_4^F(i,j,k) - m_2^F(i)m_2^F(j-k) - m_2^F(k-i) - m_2^F(k)m_2^F(i-j) \quad (3)$$

The bispectrum and cumulants obtained from the 1D sinogram are each described using 136 features; thus considering 90 different angles, each image is therefore represented with 12,240 bispectrum features and 12,240 cumulant features.

2.3.1 Elongated quinary pattern

Starting from the 2D RT image, we then applied an elongated quinary pattern (EQP) quantization technique using five levels of encoding [14]. In order to obtain elongated quinary patterns, the input image first undergoes a process in which the left-right (LR) and XY gradient magnitudes and angles are computed. To do so, gradient components are extracted using Sobel kernels in various orientations, and are then combined [15]. Therefore, for each image, one angle image (4^{th} row of Figure 3) and one magnitude image (5^{th} row of Figure 3) is calculated. Each of these images is represented by 8 coefficients (4 phase angles and 4 magnitudes – 2 XY directions and 2 LR directions). Numerous features were then derived from the magnitude and angle images. Specifically, the fuzzy entropy (Ef) [16], Kapur's entropy (Ek) [17], max entropy (Emax), Renyi's entropy (Er) [18], Shannon's entropy (ESh) [19], Vajda Entropy (Ev) [20] and Yager's entropy (Ey) [21] were extracted, and then the bispectrum entropies represented by five features were computed at every 1 degree.

Therefore, a total of 14,512 features were calculated based upon the elongated quinary pattern images. One hundred and twelve of these features were computed by considering the 8

EQP coefficients and the 7 entropies listed above, whereas the remaining 14,400 features were computed with the bispectrum entropies, from 5 features and 180 different angles.

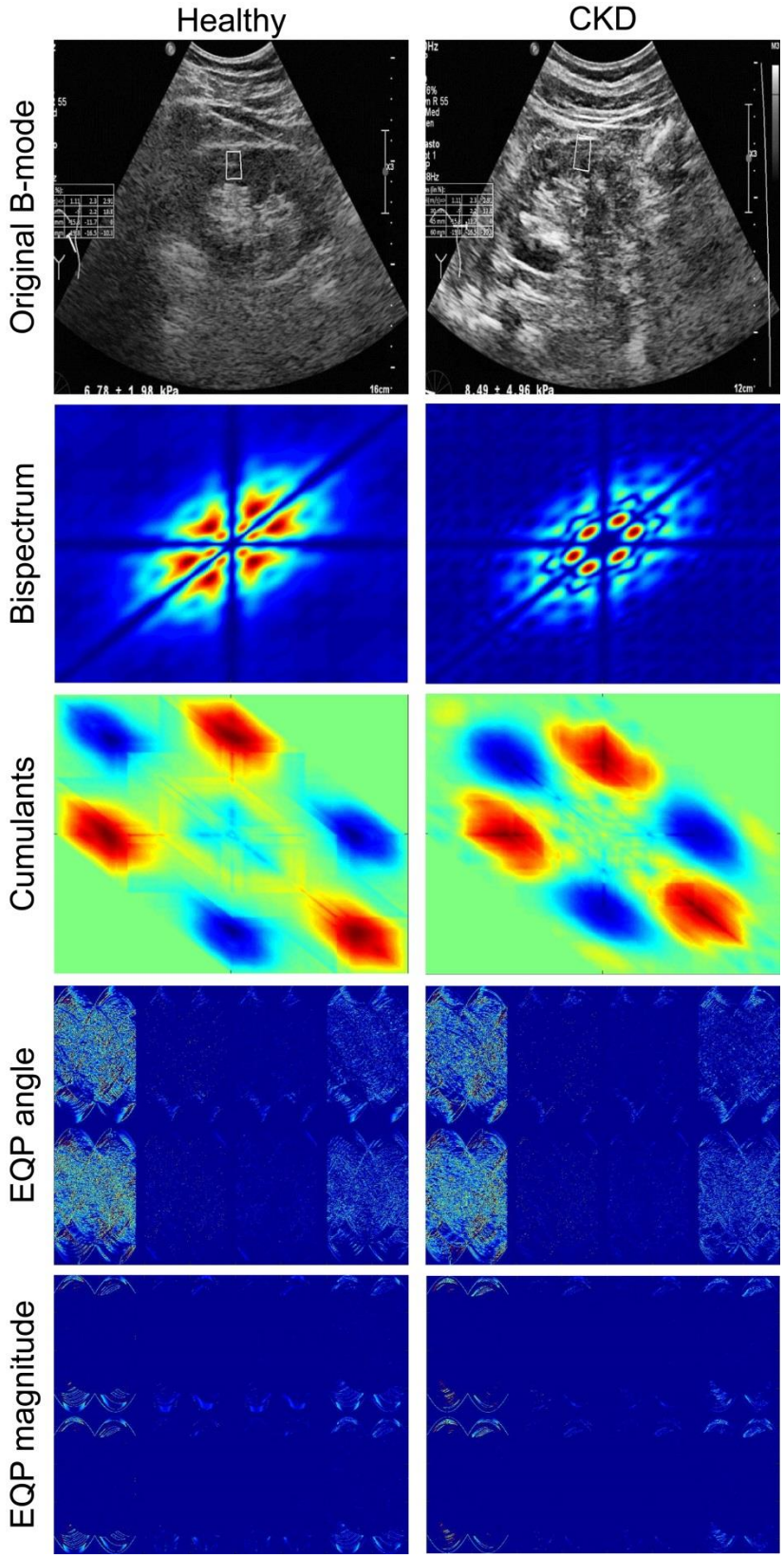

Figure 3. Example of system image processing, showing results obtained with healthy and diseased images (first and second columns, respectively). First row: Original B-mode ultrasound images of the kidney; second row: bispectrum images; third row: cumulants images; fourth row: EQP angle images; fifth row: EQP magnitude images.

2.4 Feature reduction and classification

Given that each image is over-represented with a total of 24,480 features, a feature reduction algorithm was then applied to reduce the number of image features. Specifically, a locality sensitive discriminant analysis (LSDA) approach was employed. The LSDA technique has been found helpful to study the relationship between data points; it is known to preserve both discriminant and local geometrical structure [22], and has recently been shown to be highly effective in medical image analysis [23]. For a detailed description of the functionality of the LSDA method, please refer to Cai et al. [22].

After the application of the LSDA feature reduction technique, a total of 30 features remained, which were then ranked based upon the statistical t-test, thereby providing 9 significant features.

The following methods were then employed to enable automated classification from the two-class system: k-nearest neighbour (k-NN), quadratic discriminant analysis (QDA), linear discriminant analysis (LDA), decision tree (DT), probabilistic neural network (PNN), and support vector machine (SVM). The SVM classifier can be employed using different kernel functions, and here we implemented both polynomial functions (i.e., polynomials 1, 2 and 3) and a radial basis function (RBF) [24]. For a more detailed description of these classification techniques, please refer to Acharya et al. [23].

A ten-fold cross validation strategy was utilized to train and validate the proposed algorithm. To evaluate and assess performance, the following system parameters were calculated: the accuracy, positive predictive value, sensitivity, and specificity.

3. Results

3.1 Feature extraction results

As mentioned previously, each subject is over-represented with a total of 24,480 features obtained from each image. Hence, the LSDA technique was employed to reduce 24,480 features to 30 LSDA coefficients. The LSDA coefficients were then positioned according to significance. Table 1 showcases the results of the highly ranked LSDA coefficients. Figure 4 displays a scatterplot of the two most significant LSDA coefficients, which illustrate how these features can be clearly separated, and therefore provide a satisfactory classification accuracy, which will subsequently be discussed. The results portrayed both in Figure 4 and in Table 1 show how the LSDA coefficients, extracted from the set of features, exhibit a clear distinction between subjects with and without CKD.

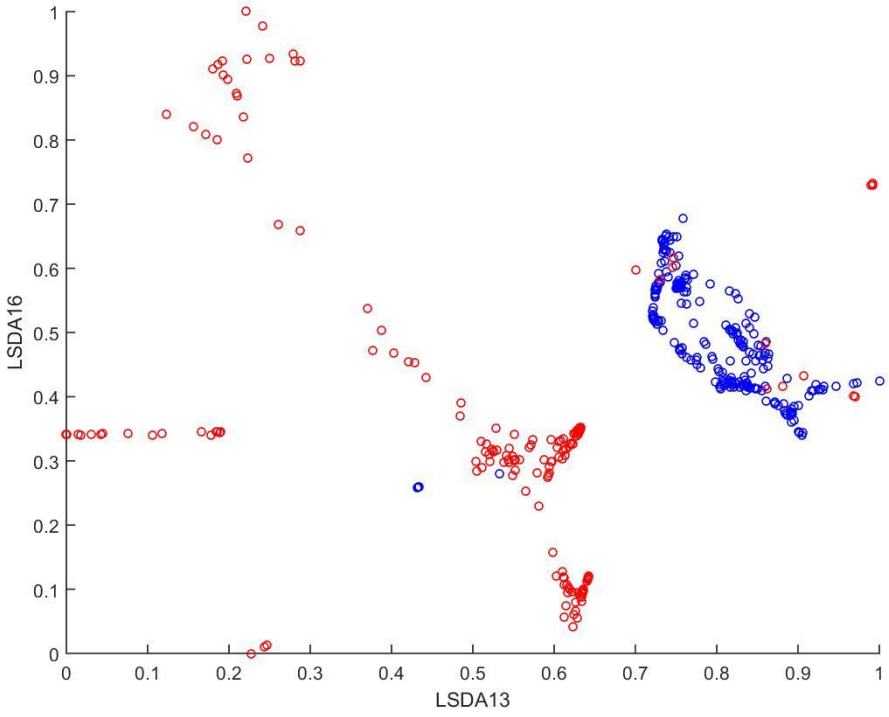

Figure 4. Scatter plot of the first and second most significant LSDA coefficients.

Table 1. Results obtained after feature reduction using LSDA.

LSDA coefficient	Normal		CKD			
	Mean	SD	Mean	SD	p-value	t-value
LSDA13	-5.91×10^{14}	1.84×10^{14}	-1.29×10^{15}	5.16×10^{14}	0.0000*	19.0087
LSDA16	4.15×10^{15}	1.84×10^{14}	3.88×10^{15}	5.10×10^{14}	0.0000*	7.3134
LSDA14	2.12×10^{15}	1.18×10^{14}	2.31×10^{15}	6.54×10^{14}	0.0000*	4.3864
LSDA12	-9.49×10^{14}	4.80×10^{13}	-7.78×10^{14}	6.59×10^{14}	0.0001*	3.9215
LSDA10	3.32×10^{14}	6.26×10^{14}	5.07×10^{14}	1.51×10^{14}	0.0004*	3.5951
LSDA9	-9.03×10^{14}	6.80×10^{13}	-1.04×10^{15}	7.60×10^{14}	0.0070*	2.7122
LSDA15	-6.62×10^{15}	6.51×10^{13}	-6.53×10^{15}	5.82×10^{14}	0.0193*	2.3488
LSDA4	-5.61×10^{15}	4.65×10^{14}	-5.53×10^{15}	2.62×10^{14}	0.0307*	2.1684
LSDA11	-9.29×10^{14}	5.40×10^{13}	-1.00×10^{15}	5.42×10^{14}	0.0422*	2.0383
LSDA8	-3.53×10^{15}	2.19×10^{14}	-3.61×10^{15}	5.94×10^{14}	0.0542	1.9311
LSDA19	-3.96×10^{15}	2.83×10^{14}	-4.04×10^{15}	5.94×10^{14}	0.0686	1.8263
LSDA3	-1.71×10^{15}	3.78×10^{13}	-1.78×10^{15}	7.47×10^{14}	0.1332	1.5048
LSDA1	-7.19×10^{15}	2.00×10^{13}	-7.23×10^{15}	6.01×10^{14}	0.2995	1.0388
LSDA18	1.22×10^{15}	1.94×10^{14}	1.19×10^{15}	5.81×10^{14}	0.4177	0.8112
LSDA2	-1.22×10^{16}	1.96×10^{13}	-1.21×10^{16}	6.08×10^{14}	0.5251	0.6361
LSDA23	9.06×10^{14}	5.10×10^{14}	9.36×10^{14}	5.53×10^{14}	0.5674	0.5723
LSDA26	5.48×10^{15}	2.58×10^{14}	5.50×10^{15}	6.04×10^{14}	0.7754	0.2855
LSDA5	4.22×10^{15}	1.05×10^{14}	4.21×10^{15}	5.94×10^{14}	0.7812	0.2780
LSDA17	-3.77×10^{15}	1.58×10^{14}	-3.76×10^{15}	6.58×10^{14}	0.7930	0.2626
LSDA27	3.93×10^{15}	3.59×10^{14}	3.94×10^{15}	5.92×10^{14}	0.8109	0.2394
LSDA20	5.69×10^{14}	4.86×10^{14}	5.64×10^{14}	5.64×10^{14}	0.9139	0.1082
LSDA28	2.52×10^{15}	4.80×10^{14}	2.51×10^{15}	2.10×10^{14}	0.9189	0.1019
LSDA22	7.05×10^{15}	5.16×10^{14}	7.05×10^{15}	3.40×10^{14}	0.9214	0.0987
LSDA30	1.09×10^{14}	3.32×10^{14}	1.05×10^{14}	5.08×10^{14}	0.9313	0.0863
LSDA25	-1.19×10^{16}	4.40×10^{14}	-1.19×10^{16}	4.05×10^{14}	0.9317	0.0857
LSDA21	1.61×10^{15}	3.50×10^{14}	1.61×10^{15}	5.24×10^{14}	0.9581	0.0526
LSDA24	-2.49×10^{15}	3.87×10^{14}	-2.48×10^{15}	5.07×10^{14}	0.9740	0.0326
LSDA7	4.31×10^{15}	1.97×10^{13}	4.31×10^{15}	7.08×10^{14}	0.9759	0.0302
LSDA6	2.42×10^{15}	1.81×10^{13}	2.42×10^{15}	6.50×10^{14}	0.9844	0.0195
LSDA29	4.81×10^{15}	2.17×10^{14}	4.81×10^{15}	6.12×10^{14}	0.9858	0.0178

*statistically significant features; LSDA: locality sensitive discriminant analysis; SD: standard deviation; CKD: chronic kidney disease.

3.2 Classification results

The final ranked features are then subject to classification using DT, LDA, QDA, k-NN, PNN, and SVM using polynomial and RBF kernel functions. The classifiers were employed singly to achieve the best classification using the least number of features. The classification

results, in terms of the confusion matrix, accuracy, positive predictive value, sensitivity, and specificity, are given in Table 2. As can be noted, the SVM using the radial basis function provided the best results with only 5 features, having an accuracy of 99.75%, a PPV equal to 99.43%, a sensitivity of 100%, and a specificity of 99.57%. These results demonstrate how the developed system was able to correctly diagnose the presence of chronic kidney disease, and only wrongly classified a normal subject as a diseased subject in 0.43% of the cases (one image was wrongly classified as a false positive).

Table 2. Classification results for chronic kidney disease determination

Classifier	N° feat.	TP	TN	FP	FN	Acc. (%)	PPV (%)	Sens. (%)	Spec. (%)
DT	8	174	228	3	0	99.26	98.31	100.00	98.70
LDA	8	167	231	0	7	98.27	100.00	95.98	100.00
QDA	5	167	224	7	7	96.54	95.98	95.98	96.97
SVM Poly 1	5	167	230	1	7	98.02	99.40	95.98	99.57
SVM Poly 2	8	171	231	0	3	99.26	100.00	98.28	100.00
SVM Poly 3	5	174	230	1	0	99.75	99.43	100.00	99.57
k-NN	4	165	227	4	9	96.79	97.63	94.83	98.27
PNN	5	171	230	1	3	99.01	99.42	98.28	99.57
SVM RBF	5	174	230	1	0	99.75	99.43	100.00	99.57

feat: features; TP: true positives; TN: true negatives; FP: false positives; FN: false negatives; Acc: accuracy; PPV: positive predictive value; Sens: sensitivity; Spec: specificity.

4. Discussion

In this study, we used a database of 405 images to develop and evaluate the performance of an automated system for distinguishing subjects with or without CKD, based upon B-mode ultrasound kidney imaging. Numerous features were extracted from each image, and the number of features was then reduced using the LSDA technique. We showed how the remaining 30 LSDA coefficients, and specifically the first five when ranked using *t-values*, were suitable and capable of automatically detecting the presence or absence of CKD. Based upon Figure 3, it can be observed that the bispectrum and cumulant plots of healthy and CKD

ultrasound images are unique. Furthermore, the EQP images (angle and magnitude) show that the healthy image displays more patterns as compared to the CKD image. Thus, a high classification performance of 99.75% was obtained with the proposed feature extraction techniques.

Additionally, the incidence of CKD has recently increased, and to remedy the concomitant financial strain, efforts to reduce the cost of managing the disease, as well as accurate CKD classification, are essential. The gold standard for the determination of CKD is the GFR/eGFR, in which CKD is categorized into 5 severity-based stages. Nearly 50 formulas have been developed to estimate the GFR since 1957 [8]. Studies have also shown that the average error of eGFR was ± 30% of the GFR [25]. In a patient with a GFR of 50 mL/ min, eGFR could vary from 35 to 65 mL/min, thereby crossing the threshold of what would define normal and abnormal GFR [26]–[28]. Regarding imaging studies, renal echogenicity can be used for evaluating the kidney, as described in the Introduction. There are four different grades of renal echogenicity, from 0 to III. However, renal damage cannot be excluded in a patient with an echogenicity grade 0 or grade I. In the assessment of kidney pathologies, the sensitivity and specificity of echogenicity grade I and grade II in detecting renal disease are 62% and 58%, respectively, while the sensitivity and specificity of echogenicity grade III are 20% and 96%, respectively [4]. These show that ultrasound kidney analysis has low sensitivity and specificity in the detection of renal damage [29, 30]. Hence, a solid and highly accurate method to determine the presence of CKD is of vital advantage for clinicians.

As mentioned in the Introduction, numerous prior investigations have focused on the correct detection of CKD. However, the majority of these studies either implemented advanced classification techniques on other clinical data obtained from each patient [5], [31]–[34], or they calculated quantitative ultrasound parameters to detect differences between healthy subjects and subjects with varying severity of CKD [6]. To the present time, no published

studies use only one B-mode ultrasound image to determine the presence or absence of CKD, an approach that can ease clinician workload, since it is necessary to acquire only a single B-mode ultrasound image for a screening test, and since it does not necessitate the collection of further clinical information.

The advantages of the method that we propose herein are therefore as follows:

- An automated classification of the presence or absence of CKD without using image segmentation techniques;
- The higher order features and EQP are able to distinguish minute variations in ultrasound images;
- High accuracy, sensitivity, and specificity. Specifically, an accuracy of 99.75%, a specificity 99.57%, and a sensitivity of 100% was determined. Therefore, no CKD subjects were incorrectly classified as healthy, and only one healthy subject was classified as having disease;
- The system is completely automated, it requires no user interaction, and only one B-mode ultrasound image is needed.

Limitations and future directions

The limitation of our work is that the database size contained only 405 subjects for evaluation. It would be necessary to test the developed technique on a larger database for applicability and diversity purposes. As a result, we did not yet render a state-of-the-art technique in this study. Nevertheless, we will develop an automated diagnostic system with deep learning in our next work. Deep learning is a highly regarded approach of artificial intelligence that eradicates the process of features extraction, selection of features, and classification. The architecture of deep learning enables the network to incorporate the conventional processes into one model [35]. It has been employed in diverse areas, from object

recognition [36] and damage assessment of high-rise building structures [37], to medical imaging [38]-[40] and physiological signals [41]-[43]. The convolutional neural network (CNN) is the most common form of deep learning [44]. The CNN paradigm entails a sequence of convolution, pooling, and fully-connected layering. Firstly, the input image is convolved with a defined kernel to produce a feature map. Through the convolution process, it singles out the characteristic features from the input. Thereafter, the pooling layer is implemented. It aims to manage overfitting of the model. Lastly, the fully-connected layer is the final output layer where class membership is determined.

In future work, we plan to design a CNN architecture with a greater number of ultrasound images (healthy and diseased) collected for study.

5. Conclusions

In this work, a novel approach using higher-order features and elongated quinary patterns, combined with the LSDA feature reduction technique, was proposed to automatically identify subjects with and without CKD using B-mode ultrasound images. Application of the developed technique resulted in an accuracy of 99.75%, a 99.43% PPV, 100% sensitivity, and 99.57% specificity with the SVM classifier and 5 features utilized. Importantly, the system exhibited excellent sensitivity, never incorrectly classifying a diseased subject as a healthy one. To the best of our knowledge, this is the first system that can automatically detect the presence or absence of CKD from ultrasound B-mode images requiring no user interaction, and can be used as a diagnostic and screening tool. Future work to be done includes enlarging the image database, further testing of the developed system, and the determination not only of the presence of CKD but also the severity of the disease.

References

[1] A. C. Webster, E. V. Nagler, R. L. Morton, and P. Masson, "Chronic Kidney Disease," *Lancet*, vol. 389, no. 10075, pp. 1238–1252, Mar. 2017.

[2] "Clinical Practice Guidelines - Management of chronic kidney disease in adults," 2011. [Online]. Available: www.acadmed.org.my/view_file.cfm?fileid=497.

[3] E. M. Remer, N. Papanicolaou, D. D. Casalino, J. T. Bishoff, M. D. Blaufox, C. A. Coursey, M. Dighe, S. C. Eberhardt, S. Goldfarb, H. J. Harvin, M. E. Heilbrun, J. R. Leyendecker, P. Nikolaidis, A. Oto, G. M. Preminger, S. S. Raman, S. Sheth, R. Vikram, and R. M. Weinfeld, "ACR Appropriateness Criteria® on Renal Failure," *Am. J. Med.*, vol. 127, no. 11, p. 1041–1048.e1, Nov. 2014.

[4] F. Fiorini and L. Barozzi, "The role of ultrasonography in the study of medical nephropathy," *J. Ultrasound*, vol. 10, no. 4, pp. 161–167, Dec. 2007.

[5] J. Norouzi, A. Yadollahpour, S. A. Mirbagheri, M. M. Mazdeh, and S. A. Hosseini, "Predicting Renal Failure Progression in Chronic Kidney Disease Using Integrated Intelligent Fuzzy Expert System," *Comput. Math. Methods Med.*, vol. 2016, pp. 1–9, Feb. 2016.

[6] J. Gao, A. Perlman, S. Kalache, S. Seshan, L. Smith, and J. Chevalier, "Multiparametric Quantitative Ultrasound Imaging to Assess Chronic Kidney Disease," in *Ultrasound in Medicine & Biology*, 2017, vol. 43, p. S209.

[7] S. S. Leong, J. H. D. Wong, M. N. Md Shah, A. Vijayananthan, M. Jalalonmuhali, and K. H. Ng, "Shear wave elastography in the evaluation of renal parenchymal stiffness in patients with chronic kidney disease," *Br. J. Radiol.*, p. 20180235, Jun. 2018.

[8] A. E. Samir, A. S. Allegretti, Q. Zhu, M. Dhyani, A. Anvari, D. A. Sullivan, C. A. Trottier, S. Dougherty, W. W. Williams, J. L. Babitt, J. Wenger, R. I. Thadhani, and H. Y. Lin, "Shear wave elastography in chronic kidney disease: a pilot experience in native kidneys," *BMC Nephrol.*, vol. 16, no. 1, p. 119, Dec. 2015.

[9] S. M. Pizer, E. P. Amburn, J. D. Austin, R. Cromartie, A. Geselowitz, T. Greer, B. ter Haar Romeny, J. B. Zimmerman, and K. Zuiderveld, "Adaptive histogram equalization and its variations," *Comput. Vision, Graph. Image Process.*, vol. 39, no. 3, pp. 355–368, Sep. 1987.

[10] J. Radon, "On the determination of functions from their integral values along certain manifolds," *IEEE Trans. Med. Imaging*, vol. 5, no. 4, pp. 170–176, Dec. 1986.

[11] C. L. Nikias and M. R. Raghuveer, "Bispectrum estimation: A digital signal processing framework," *Proc. IEEE*, vol. 75, no. 7, pp. 869–891, 1987.

[12] R. J. Martis, U. R. Acharya, K. M. Mandana, A. K. Ray, and C. Chakraborty, "Cardiac decision making using higher order spectra," *Biomed. Signal Process. Control*, vol. 8, no. 2, pp. 193–203, Mar. 2013.

[13] R. J. Martis, U. R. Acharya, C. M. Lim, K. M. Mandana, A. K. Ray, and C. Chakraborty, "Application of Higher Order Cumulant Features for Cardiac Health Diagnosis Using Ecg Signals," *Int. J. Neural Syst.*, vol. 23, no. 04, p. 1350014, 2013.

[14] S. A. M. Al-Sumaidaee, M. A. M. Abdullah, R. R. O. Al-Nima, S. S. Dlay, and J. A. Chambers, "Multi-gradient features and elongated quinary pattern encoding for image-based facial expression recognition," *Pattern Recognit.*, vol. 71, pp. 249–263, Nov. 2017.

[15] U. Raghavendra, A. Gudigar, M. Maithri, A. Gertych, K. M. Meiburger, C. H. Yeong, C. Madla, P. Kongmebhol, F. Molinari, K. H. Ng, and U. R. Acharya, "Optimized

multi-level elongated quinary patterns for the assessment of thyroid nodules in ultrasound images," *Comput. Biol. Med.*, vol. 95, 2018.

[16] Weiting Chen, Zhizhong Wang, Hongbo Xie, and Wangxin Yu, "Characterization of Surface EMG Signal Based on Fuzzy Entropy," *IEEE Trans. Neural Syst. Rehabil. Eng.*, vol. 15, no. 2, pp. 266–272, Jun. 2007.

[17] J. N. Kapur, P. K. Sahoo, and A. K. C. Wong, "A new method for gray-level picture thresholding using the entropy of the histogram," *Comput. Vision, Graph. Image Process.*, vol. 29, no. 3, pp. 273–285, Mar. 1985.

[18] A. Renyi, "On measures of Entropy and Information," in *Fourth Berkeley Symposium on Mathematical Statistics and Probability, Volume 1: Contributions to the Theory of Statistics*, 1961, pp. 547–561.

[19] C. E. Shannon and C. E., "A mathematical theory of communication," *ACM SIGMOBILE Mob. Comput. Commun. Rev.*, vol. 5, no. 1, pp. 3–55, Jan. 2001.

[20] V. Pandey and V. Gupta, "MRI Image Segmentation Using Shannon and Non Shannon Entropy Measures," *Int. J. Appl. or Innov. Eng. Manag.*, vol. 3, no. 7, pp. 41–46, 2014.

[21] Q. HU and D. YU, "ENTROPIES OF FUZZY INDISCERNIBILITY RELATION AND ITS OPERATIONS," *Int. J. Uncertainty, Fuzziness Knowledge-Based Syst.*, vol. 12, no. 05, pp. 575–589, Oct. 2004.

[22] D. Cai, X. He, K. Zhou, J. Han, and H. Bao, "Locality Sensitive Discriminant Analysis," in *20th International Joint Conference on Artificial Intelligence*, 2007, pp. 708–713.

[23] U. R. Acharya, U. Raghavendra, H. Fujita, Y. Hagiwara, J. E. Koh, T. Jen Hong, V. K. Sudarshan, A. Vijayananthan, C. H. Yeong, A. Gudigar, and K. H. Ng, "Automated characterization of fatty liver disease and cirrhosis using curvelet transform and entropy features extracted from ultrasound images," *Comput. Biol. Med.*, vol. 79, no. June, pp. 250–258, 2016.

[24] R. Duda, P. Hart, and D. Stork, *Pattern classification*. 2012.

[25] S. Luis-Lima and E. Porrini, "An Overview of Errors and Flaws of Estimated GFR versus True GFR in Patients with Diabetes Mellitus.," *Nephron*, vol. 136, no. 4, pp. 287–291, 2017.

[26] A. J. Wood, L. Churilov, N. Perera, D. Thomas, A. Poon, R. J. MacIsaac, G. Jerums, and E. I. Ekinci, "Estimating glomerular filtration rate: Performance of the CKD-EPI equation over time in patients with type 2 diabetes," *J. Diabetes Complications*, vol. 30, no. 1, pp. 49–54, Jan. 2016.

[27] P. Rossing, K. Rossing, P. Gaede, O. Pedersen, and H.-H. Parving, "Monitoring kidney function in type 2 diabetic patients with incipient and overt diabetic nephropathy.," *Diabetes Care*, vol. 29, no. 5, pp. 1024–30, May 2006.

[28] N. Fontseré, I. Salinas, J. Bonal, B. Bayés, J. Riba, F. Torres, J. Rios, A. Sanmartí, and R. Romero, "Are prediction equations for glomerular filtration rate useful for the long-term monitoring of type 2 diabetic patients?," *Nephrol. Dial. Transplant.*, vol. 21, no. 8, pp. 2152–2158, Aug. 2006.

[29] G. Zamir, W. Sakran, Y. Horowitz, A. Koren, and D. Miron, "Urinary tract infection: is there a need for routine renal ultrasonography?," *Arch. Dis. Child.*, vol. 89, no. 5, pp. 466–8, May 2004.

[30] H. Lee, B. Hyun Soh, C. Hee Hong, M. Joon Kim, and S. Won Han, "The efficacy of ultrasound and dimercaptosuccinic acid scan in predicting vesicoureteral reflux in children below the age of 2 years with their first febrile urinary tract infection," *Pediatr. Nephrol.*, vol. 24, no. 10, pp. 2009–2013, Oct. 2009.

[31] V. Kunwar, K. Chandel, A. S. Sabitha, and A. Bansal, "Chronic Kidney Disease analysis using data mining classification techniques," in *2016 6th International*

Conference - Cloud System and Big Data Engineering (Confluence), 2016, pp. 300–305.

[32] L. Jena and N. K. Kamila, "Distributed Data Mining Classification Algorithms for Prediction of Chronic-Kidney-Disease," *Int. J. Emerg. Res. Manag. &Technology*, no. 11, pp. 2278–9359, 2015.

[33] S. Vijayarani and M. S. Dhayanand, "Kidney disease prediction using SVM and ANN algorithms," *Int. J. Comput. Bus. Res.*, vol. 6, no. 2, 2015.

[34] P. Sinha and P. Sinha, "Comparative Study of Chronic Kidney Disease Prediction using KNN and SVM," *Int. J. Eng. Res. Technol.*, vol. 4, no. 12, pp. 608–612, 2015.

[35] O. Faust, Y. Hagiwara, J. H. Tan, S. L. Oh, and U. R. Acharya, "Deep learning for healthcare applications based on physiological signals: a review," *Computer Methods and Programs in Biomedicine*, vol. 161, pp. 1-13, July 2018.

[36] A. Krizhevsky, I. Sutskever, G. E. Hinton, "ImageNet classification with deep convolutional neural networks," *Proceedings of the 25th International Conference on Neural Information Processing Systems – Volume 1*, Lake Tahoe, Nevada, pp. 1097-1105, 2012.

[37] M. H. Rafiei and H. Adeli, "A novel machine learning based algorithm to detect damage in highrise building structures," *The Structural Design of Tall and Special Buildings,* vol. 26, no. 18, 2017, DOI: 10.1002/tal.1400.

[38] J. H. Tan, S. V. Bhandary, S. Sivaprasad, Y. Hagiwara, A. Bagchi, U. Raghavendra, A. K. Rao, B. Raju, N. S. Shetty, A. Gertych, K. C. Chua, U. R. Acharya, "Age-related macular degeneration detection using deep convolutional neural network," *Future Generation Computer Systems*, vol. 87, pp. 127-135, 2018.

[39] J. G. Lee, S. Jun, Y. W. Cho, H. Lee, G. B. Kim, J. B. Seo, N. Kim, "Deep learning in medical imaging: general overview," Korean Journal of Radiology, vol. 18, no. 4, pp. 570-584, 2017.

[40] U. Raghavendra, N. S. Bhat, A. Gudigar, U. R. Acharya, "Automated system for the detection of thoracolumbar fractures using a CNN architecture," *Future Generation Computer Systems*, vol. 85, pp. 184-189, 2018.

[41] U. R. Acharya, H. Fujita, S. L. Oh, Y. Hagiwara, J. H. Tan, M. Adam, R. S. Tan, "Deep convolutional neural network for the automated diagnosis of congestive heart failure using ECG signals," *Applied Intelligence*, Springer US, pp. 1-12, 2018.

[42] J. H. Tan, Y. Hagiwara, W. Pang, I. Lim, S. L. Oh, M. Adam, R. S. Tan, M. Chen, U. R. Acharya, "Application of stacked convolutional and long short-term memory network for accurate identification of CAD ECG signals," *Computers in Biology and Medicine*, vol. 94, pp. 19-26, 2018.

[43] U. R. Acharya, S. L. Oh, Y. Hagiwara, J. H. Tan, H. Adeli, D. P. Subha, "Automated EEG-based screening of depression using deep convolutional neural network," *Computer Methods and Programs in Biomedicine*, vol. 161, pp. 103-113, 2018.

[44] Y. LeCun, Y. Bengio, G. Hinton, "Deep learning," *Nature*, vol. 521, pp. 436-444, 2015.